11-11-2015

In vivo evaluation of adipose-derived stromal cells delivered with a nanofiber scaffold for tendon-to-bone repair

Justin Lipner
Washington University School of Medicine

Hua Shen
Washington University School of Medicine

Leonardo Cavinatto
Washington University School of Medicine

Wenying Liu
Georgia Institute of Technology

Necat Havlioglu
John Cochran VA Medical Center

See next page for additional authors

TISSUE ENGINEERING: Part A
Volume 21, Numbers 21 and 22, 2015

DOI: 10.1089/ten.tea.2015.0101

termis
Tissue Engineering
& Regenerative Medicine
International Society

ORIGINAL ARTICLE

In Vivo Evaluation of Adipose-Derived Stromal Cells Delivered with a Nanofiber Scaffold for Tendon-to-Bone Repair

Justin Lipner, PhD,[1,2] Hua Shen, PhD,[1] Leonardo Cavinatto, MD,[1] Wenying Liu, PhD,[3]
Necat Havlioglu, MD,[4] Younan Xia, PhD,[5] Leesa M. Galatz, MD,[1] and Stavros Thomopoulos, PhD[6]

Rotator cuff tears are common and cause a great deal of lost productivity, pain, and disability. Tears are typically repaired by suturing the tendon back to its bony attachment. Unfortunately, the structural (e.g., aligned collagen) and compositional (e.g., a gradient in mineral) elements that produce a robust attachment in the healthy tissue are not regenerated during healing, and the repair is prone to failure. Two features of the failed healing response are deposition of poorly aligned scar tissue and loss of bone at the repair site. Therefore, the objective of the current study was to improve tendon-to-bone healing by promoting aligned collagen deposition and increased bone formation using a biomimetic scaffold seeded with pluripotent cells. An aligned nanofibrous poly(lactic-*co*-glycolic acid) scaffold with a gradient in mineral content was seeded with adipose-derived stromal cells (ASCs) and implanted at the repair site of a rat rotator cuff model. In one group, cells were transduced with the osteogenic factor bone morphogenetic protein 2 (BMP2). The healing response was examined in four groups (suture only, acellular scaffold, cellular scaffold, and cellular BMP2 scaffold) using histologic, bone morphology, and biomechanical outcomes at 14, 28, and 56 days. Histologically, the healing interface was dominated by a fibrovascular scar response in all groups. The acellular scaffold group showed a delayed healing response compared to the other groups. When examining bone morphology parameters, bone loss was evident in the cellular BMP2 group compared to other groups at 28 days. When examining repair-site mechanical properties, strength and modulus were decreased in the cellular BMP2 groups compared to other groups at 28 and 56 days. These results indicated that tendon-to-bone healing in this animal model was dominated by scar formation, preventing any positive effects of the implanted biomimetic scaffold. Furthermore, cells transduced with the osteogenic factor BMP2 led to impaired healing, suggesting that this growth factor should not be used in the tendon-to-bone repair setting.

Introduction

ROTATOR CUFF TEARS are common, particularly in the aging population, and lead to significant lost productivity, pain, and disability. In the United States, ~600,000 patients require rotator cuff-related surgery each year.[1] Unfortunately, a large number of surgical repairs fail, even in the young and healthy patient population.[2] At the root of these failures is a healing process of tendon to bone that does not regenerate the original tissue and is characterized by bone loss and scar formation.[3] At the healing interface, a lack of graded mineral content and poorly organized collagen fibers result in a mechanically weak attachment.[4,5] The poor results after rotator cuff repair in the clinical population motivate the need for novel approaches to enhance healing and improve outcomes.

Two key features of poor healing, and hence therapeutic targets, are mineral loss in the bone adjacent to the tendon attachment and poorly organized collagen deposition at the repair site.[6,7] Bone loss is a well-described outcome of tendon-to-bone healing. Loss of bone occurs after tendon and ligament tears, presumably due to the loss of mechanical loading.[8] However, significant bone loss is also apparent when surgical repair is performed soon after injury.[6] This

Departments of [1]Orthopedic Surgery and [2]Biomedical Engineering, Washington University in St. Louis, St. Louis, Missouri.
[3]School of Chemical and Biomolecular Engineering, Georgia Institute of Technology, Atlanta, Georgia.
[4]Department of Pathology, John Cochran VA Medical Center, St. Louis, Missouri.
[5]The Wallace H. Coulter Department of Biomedical Engineering, Georgia Institute of Technology, Atlanta, Georgia.
[6]Department of Orthopedic Surgery, Columbia University, New York, New York.

post-repair bone loss is thought to be the result of increased osteoclast activity in the bone directly adjacent to the attachment.[9] Furthermore, suppression of bone resorption results in improved healing.[10] Less is known about the effect of bone anabolic agents (e.g., bone morphogenetic protein 2 [BMP2]) on tendon-to-bone healing.[11,12] A second feature of tendon-to-bone healing is the deposition of disorganized extracellular matrix rather than the well-aligned collagen fibers found in native tendon.[7] This scar tissue is an order-of-magnitude weaker than the uninjured tissue and is not well integrated into the bone.[7] Enhanced bone formation and aligned collagen deposition integrating across the attachment would greatly enhance the strength of the healing interface.

Based on these prior observations, the goal of the current study was to enhance tendon-to-bone healing by delivery of an aligned biomimetic scaffold with pluripotent cells and an osteogenic factor (BMP2) to the repair site. This scaffold mimicked two features that are critical to the mechanics of the natural tendon-to-bone attachment: aligned fibers and a gradient in mineral content.[13,14] In support of this approach, *in vitro* experiments showed that a gradient in mineral led to a gradient in osteogenesis by adipose-derived stromal cells (ASCs).[15] We hypothesized that (i) aligned nanofibers would guide deposition of aligned collagen, (ii) a mineral gradient would promote graded differentiation of the implanted stromal cells, and (iii) BMP2 would promote osteogenesis and bone formation at the repair site. The combination of improved collagen orientation and increased bone formation was expected to result in a stronger and tougher tendon-to-bone repair.

Materials and Methods

Study design

To examine the effects of scaffold characteristics (alignment and mineral content), ASCs, and BMP2 on tendon-to-bone healing, four groups were examined in a rat rotator cuff injury and repair model: suture repair (i.e., without ASCs or scaffold), acellular scaffold (i.e., repair with scaffold, but without ASCs), cellular scaffold (i.e., repair with ASC-seeded scaffold), and cellular BMP2 scaffold (i.e., repair with BMP2-transduced ASC-seeded scaffold). Repairs were evaluated at 14, 28, and 56 days for histologic, morphologic, and biomechanical outcomes.

Cell-seeded layered scaffold

A multilayered scaffold was used to deliver structural (i.e., aligned nanofibers), compositional (i.e., spatial gradient in mineral), and biologic (i.e., BMP2 produced by ASCs) cues to the repair site. This layered design followed a similar approach previously developed for flexor tendon repair.[16] The implanted scaffold had five layers: three sheets of poly(lactic-*co*-glycolic acid) (PLGA) nanofibers with gradients in mineral with two layers of fibrin matrix between them. The fibrin provided a rapidly resorbed layer with a large enough volume to deliver cells to the repair site.

PLGA nanofiber mat with spatial gradient of mineral content. Nonwoven mats of nanofibers were generated by electrospinning PLGA (85:15 lactic:glycolic ratio; Sigma, St. Louis, MO) onto conducting collectors, as described previously.[14] The fiber diameters were 400–900 nm (as measured using scanning electron microscopy [SEM] images), and the fiber mats were $\sim$60-μm thick (as measured by laser micrometer, LK-081; Keyence, Osaka, Japan). The electrospun scaffolds were then mineralized with a gradient in mineral by a 10 times simulated body fluid (10SBF).[17] To prepare the scaffolds for mineralization, the samples were cut into pieces and mounted onto carbon tape-covered wire frames. The mounted samples were then plasma treated for 8 min to increase surface energy and hydrophillicity (PDC-001; Harrick Plasma, Ithaca, NY).[18] Scaffolds were soaked in 10SBF without sodium bicarbonate for 30 min to bind calcium to the surface. The mounted samples were then placed in glass vials and filled with 10SBF. A syringe pump was used to fill the vials at a constant rate to create linear gradients in immersion time and hence mineral content.[14]

SEM was used to verify the fiber and mineral morphologies. Samples were mounted on carbon tape-coated aluminum SEM posts and sputter coated with Au-Pd for $\sim$45 s to allow a charge path for the primary electrons. Posts were then imaged under high vacuum using an FEI Nova NanoSEM 2300 and accelerating voltages of between 5 and 10 kV. An energy-dispersive X-ray was performed using the FEI Nova NanoSEM 2300 during SEM imaging to determine the spatial variation of mineral content along the length of the scaffold. Moving in 1–2 mm increments, regions were assessed for their calcium and carbon atomic content. Three regions were analyzed for each measurement along the mineral gradient and averaged for atomic content. Three 5-$\times$5-mm scaffold pieces were used to create the final five-layer construct, as described previously.[16] All scaffolds had appropriate fiber diameters and mineral gradients, consistent with our previous work.[14]

Fibrin hydrogel. Fibrin solution was prepared from human fibrinogen (EMD Millipore, Billerica, MA) and dissolved in tris-buffered saline at a concentration of 20 mg/mL. The fibrin solution was filtered and combined 1:1 with three components to produce the polymerizing fibrin solution: 140 parts alpha-minimum essential medium, 55 parts 50 mM $CaCl_2$, and 5 parts 1000 U/mL thrombin. Constructs were assembled from three layers of PLGA, joined by two layers of fibrin hydrogel that adhered the layers together and provided volume to deliver a large amount of cells.[16] Cellular gels were created with identical fibrin mixed with 3.6 million cells. The final scaffolds measured roughly $5\times5\times1$ mm, leading to a cell concentration of $\sim$2 million cells per milliliter (500,000 cells/scaffold).

Adipose-derived stromal cells. Allogeneic ASCs were isolated from the subcutaneous adipose tissue of juvenile male Sprague-Dawley rats. The tissue was digested using 0.2% collagenase A for 2 h, and the resulting cell solution was passed through 70-μm filters, cultured, and selected for plastic adherence. Cellular scaffolds were seeded with passage 3 cells overnight at a density of 35,000/cm^2 before implantation. These cells have been shown to be able to differentiate into a wide variety of lineages, including tenocytes, chondrocytes, and osteoblasts.[19,20]

Generation and testing of human BMP2-yellow fluorescent protein construct and adenovirus. For delivery of BMP2,

cells were transduced with an adenovirus that leads them to produce a BMP2-yellow fluorescent protein (YFP) fusion protein. To create viral vectors, a human (h) BMP2 construct (kindly provided by Dr. Su-Li Cheng at Washington University in St. Louis) without a stop code was cloned into a pCR2.1 vector by polymerase chain reaction (PCR) cloning. To generate the recombinant hBMP2-YFP construct, a YFP construct with a stop code at the 3′ end of its coding sequence and *Eco*RV and *Not*I restriction sites at its 5′ and 3′ ends, respectively, was generated by PCR and cloned into pCR2.1-hBMP2 vector at *Eco*RV and *Not*I sites, with its 5′ end in frame with the hBMP2 coding sequence. The resulting hBMP2-YFP construct was subsequently cloned into a pVQpacAd5CMVK-NpA shuttle vector (ViraQuest, Inc., North Liberty, IA) at *Kpn*I and *Not*I sites. The hBMP2-YFP adenovirus was commercially prepared and purified to 5×10^{10} plaque-forming units/mL (ViraQuest). Titration tests were used to test the effectiveness of different vector concentrations (0, 0.25, 0.5, 1, 2, 4 μL of vector solution) and changes in BMP2 expression over time (Supplementary Fig. S1; Supplementary Data are available online at www.liebertpub.com/tea). Based on these *in vitro* studies, 4 μL vector per 500,000 cells concentration and 3 days of culture were chosen for cells implanted *in vivo*.

Surgical procedure

Sixty-four Sprague-Dawley male rats were used for this study (Jackson Labs, Bar Harbor, ME). All procedures were approved by the Animal Studies Committee at Washington University. Animals were anesthetized using isoflurane, and surgeries were performed under sterile conditions. The supraspinatus tendon was cut cleanly from its attachment to the humeral head. A burr was used to remove existing fibrocartilage at the attachment footprint. The tendon was grasped with a modified Mason Allen stitch and passed through a bone tunnel in the humeral head. Four groups were examined: suture repair, acellular scaffold, cellular scaffold, and cellular BMP2 scaffold.

In the groups with scaffolds, a 5-×5-mm scaffold was placed over the repair site, with three suture attachment points: tendon suture, periosteum distal to the repair site, and supraspinatus muscle proximal to the repair site (Fig. 1). Postoperatively, animals were allowed free cage activity. Animals were randomized to sacrifice timepoints of 14, 28, or 56 days and assayed for bone morphometry and biomechanics ($N=8$–10 per group), or histology ($N=2$–4 per group).

Bone morphometry

Samples were scanned in air using microcomputed tomography (microCT) (SCANCO μCT40) with 20 μm resolution and 300 ms integration time at 45 kV/177 μA. Two different volumes were analyzed: the scar over the repair site and the trabecular bone of the humeral head. Scar characteristics were determined for a 4-mm region near the tendon-to-bone attachment of the supraspinatus tendon, using thresholds between 70 and 240. Trabecular bone morphometry was measured in a volume of interest spanning ~2.5 mm between the growth plate and the epiphyseal surface, excluding the cortical bone. Bone morphometry parameters were calculated using the manufacturer's software (Scanco, Brüttisellen, Switzerland), including bone volume fraction (BV/TV), bone mineral density (BMD), and trabecular architecture (thickness [Tb.Th.], number [Tb.N.], and separation [Tb.S.]).

Mechanical testing and analysis

Uniaxial tensile tests were performed using an Instron 5866 (Instron, Norwood, MA) with custom grips and analyzed using a custom code written in MATLAB (Mathworks, Natick, MA). Samples were tested at quasi-static conditions, with a stress relaxation of 5 min followed by a test to failure at a constant strain rate of ~0.1%/s. A video was captured concurrently at 2 fps with a resolution of 3296×2474 pixels (VMV-8M; Illunis, Minnetonka, MN). Engineering stress was calculated by dividing force by the initial cross-sectional area. Strain was determined as change in length divided by original length. Length-deformation data were analyzed to find the stiffness (slope of the linear region of the force-displacement curve), maximum force,

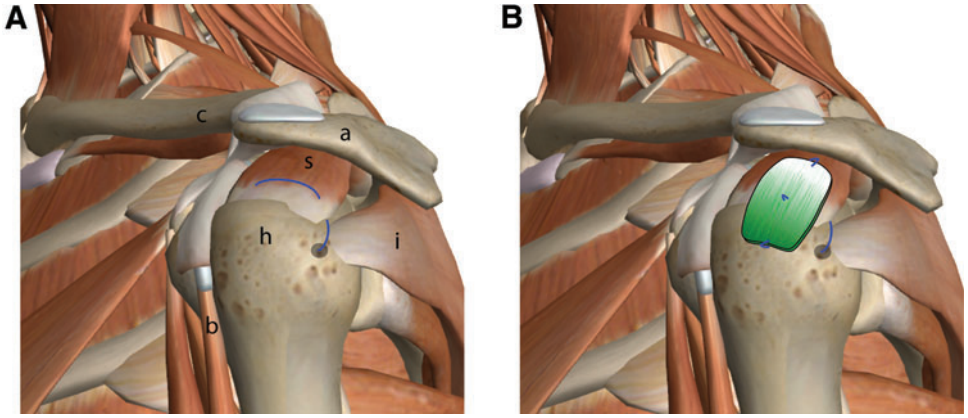

FIG. 1. A schematic of the human shoulder is shown **(A)** with the proposed placement of the scaffold **(B)**. In the current study, the rat supraspinatus tendon was injured and repaired in a similar fashion, with the scaffold placed over the repair site. The mineralized end was placed over the bone, and the unmineralized was placed over the tendon (mineral content indicated by *green* shading in **B**). Repair sutures are shown in *blue*. s, supraspinatus muscle; a, acromion; h, humeral head; i, infraspinatus muscle; b, biceps tendon; images modified from ZygoteBody. Color images available online at www.liebertpub.com/tea

yield load, and yield deformation. Stress–strain data were analyzed to find the modulus (slope of the linear region of the stress–strain curve), strength (maximum stress), yield stress, yield strain, and toughness.

Histology

Samples selected for histology were demineralized in ethylenediaminetetraacetic acid and then processed for either frozen or paraffin-embedded sections. Samples in the suture and cellular BMP2 groups were first embedded in frozen Optimal Cutting Temperature (Tissue-Tek®; VWR, Radnor, PA) to avoid autofluorescence of the paraffin that would obscure visualization of the BMP2-YFP. Frozen samples were cryosectioned at 8 μm and stained with DAPI to visualize nuclei. After collecting frozen sections, the samples were reembedded in paraffin. Samples in the other two groups were only embedded in paraffin. Paraffin-embedded samples were sectioned at 8 μm and stained with trichrome, safranin O/fast green, toluidine blue, or hematoxylin/eosin. Histologic sections were graded blindly by Necat Havlioglu for cellularity, inflammation, and tendon-to-bone healing according to the maturity scale described by Yokoya *et al.* (for details on scoring, see legend of Table 1).[21]

Statistics

Mechanical data were excluded from the final dataset if grip slippage (9 out of 88 samples) or growth plate failure (7 out of 88 samples) occurred. To compare mechanical and microCT outcomes, a two-way analysis of variance was performed on two factors (time: 28, 56 days; and treatment: suture, acellular, cellular, cellular BMP2), followed by Fisher's least-squared difference *post hoc* tests for time, treatment, and combined time and treatment effects. Statistical significance was set at an α level of 0.05. Histologic scores were not statistically compared due to their semi-quantitative nature.

Results

BMP2 transduction and in vivo *delivery*

In vitro culture of BMP2-transduced ASCs showed that 4 μL of the virus was effective for BMP2 production after 24 h (Supplementary Fig. S1A). Expression increased over the first 3 days of culture and plateaued thereafter (Supplementary Fig. S1B). Based on these results, a 3 day culture period was chosen between incubation and implantation *in vivo*. Delivery of BMP2 to the repair site was validated by observation of YFP in histologic sections at 28 and 56 days after surgical repair (Supplementary Fig. S1C).

Histology

The healing interface was dominated by fibrovascular scar in all groups (Fig. 2 and Supplementary Fig. S2 and Table 1), as evidenced by high cellularity and vascularity, and poor collagen orientation and insertion site continuity. The scar was remodeled over time, as indicated by histologic scores improving toward normal by 56 days. When comparing the four groups, the groups that contained a scaffold showed a notably delayed healing response compared to the suture-only group. Specifically, scores for cellularity, fraction of

Table 1. Histologic Scores for Repair Groups at 14, 28, and 56 Days

	14 days	*28 days*				*56 days*			
	Acellular	*Suture*	*Acellular*	*Cellular*	*BMP2*	*Suture*	*Acellular*	*Cellular*	*BMP2*
Cellularity	3.5 (2, 4)	1 (1, 1)	3 (2, 3)	2 (2, 3)	2 (1, 3)	2 (1, 3)	3 (3, 3)	2 (2, 2)	2.5 (2, 3)
Fibroblasts	2.5 (1, 4)	1 (1, 1)	2 (1, 3)	3 (2, 3)	1.5 (1, 3)	2 (1, 3)	2 (2, 2)	1.5 (1, 2)	2 (1, 3)
Vascularity	3 (2, 4)	3 (3, 3)	2 (2, 3)	2 (2, 3)	3 (2, 4)	2 (2, 2)	2.5 (2, 3)	2.5 (2, 3)	3.5 (3, 4)
Matrix	3 (2, 4)	1.5 (1, 3)	2 (2, 3)	3 (2, 3)	2 (2, 3)	2 (1, 3)	2 (2, 2)	2 (2, 2)	1.5 (1, 2)
Cell orient	3 (1, 4)	1.5 (1, 2)	2 (2, 2)	2 (2, 3)	2 (2, 3)	1.5 (1, 2)	2 (2, 2)	2 (2, 2)	1.5 (1, 2)
Coll. orient	4 (2, 4)	2 (2, 2)	3 (3, 3)	3 (2, 3)	2.5 (1, 3)	2.5 (2, 3)	2 (2, 2)	2.5 (2, 3)	2 (2, 2)
Ins. histo.	3.5 (2, 4)	2 (1, 3)	3 (3, 3)	3 (1, 3)	2.5 (1, 3)	3 (2, 4)	2 (2, 2)	3 (3, 3)	2 (2, 2)
Ins. cont.	4 (2, 4)	2 (2, 3)	3 (3, 3)	3 (2, 3)	2.5 (1, 3)	2.5 (2, 3)	2 (2, 2)	2.5 (2, 3)	2 (2, 2)
Maturity	26.5 (14, 32)	14.5 (12, 17)	20 (19, 22)	22 (15, 23)	18 (12, 24)	17.5 (12, 23)	17.5 (17, 18)	18 (17, 19)	17 (14, 20)

Each outcome was scored from 1 (closest to normal) to 4 (most abnormal). The sum of scores was used as an indication of enthesis maturity (8: normal, 32: furthest from normal). Specifically, cellularity (4: high, 1: low), fibroblasts (4: <25% of total, 3: 26–50%, 2: 51–75%, 1: >75%), vascularity (4: 15 bv/low PF, 3: 11–15 bv/low PF, 2: 6–10 bv/low PF, 1: <6 bv/low PF), matrix (4: minimal, 1: marked), cells parallel (4: <25%, 3: 26–50%, 2: 51–75%, 1: >75%), collagen orientation (4: <25% fibers parallel, 3: 26–50%, 2: 51–75%, 1: >75%), insertion histological findings (4: lacks fibrocartilage/regularity/tidemark, 3: regularity but lacks fibrocartilage/tidemark, 2: regularity and fibrocartilage but lacks tidemark, 1: regularity/fibrocartilage/tidemark present), insertion continuity (4: <25%, 3: 26–50%, 2: 51–75%, 1: >75%). Data are presented as median (range).
BMP2, bone morphogenetic protein 2; bv, blood vessels; PF, power field.

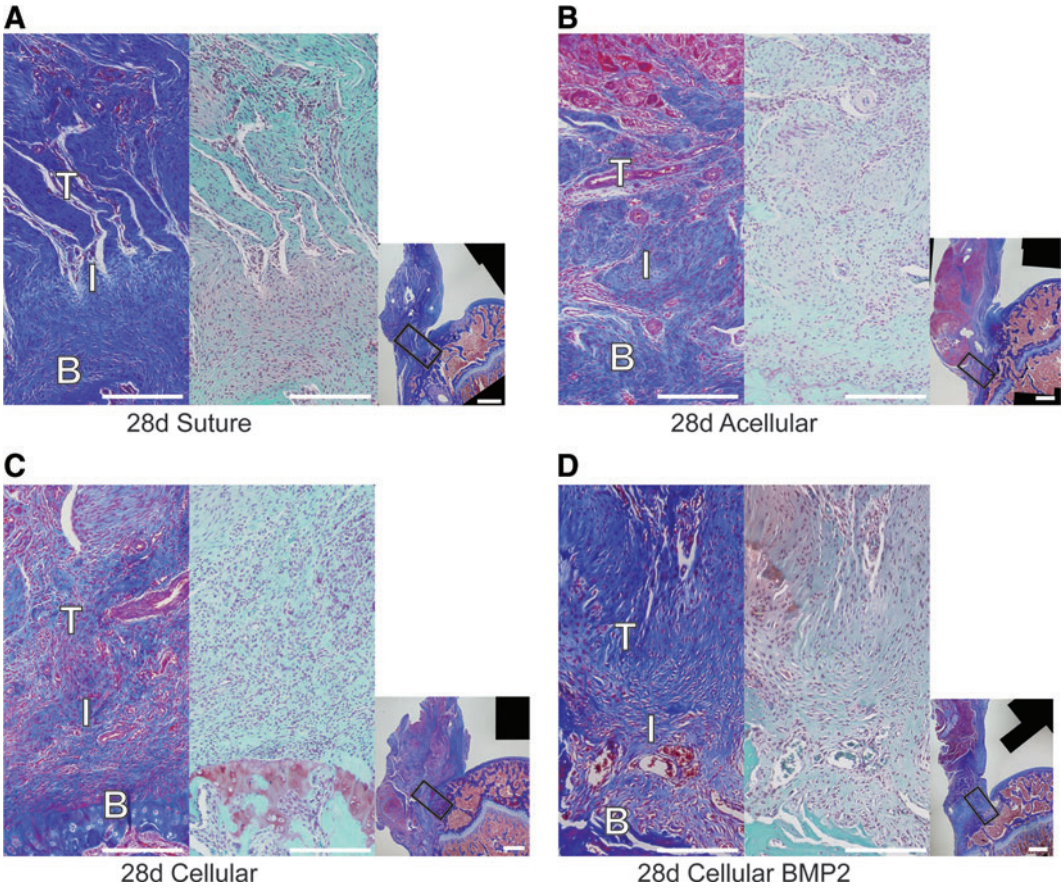

FIG. 2. Representative histology images from groups at 28 days. For each *panel* **(A)** suture group, **(B)** acellular group, **(C)** cellular group, and **(D)** cellular BMP2 group, high magnification views are shown on the *left* (trichrome stain) and *center* (safranin O stain), and a low magnification view (trichrome) is shown on the *right*. *Rectangles* in the low magnification views denote the positions of the high magnification views. T, tendon; I, insertion; B, bone. Scale bars = 0.5 mm in high magnification *panels*, 1 mm in low magnification *panels*. Color images available online at www.liebertpub.com/tea

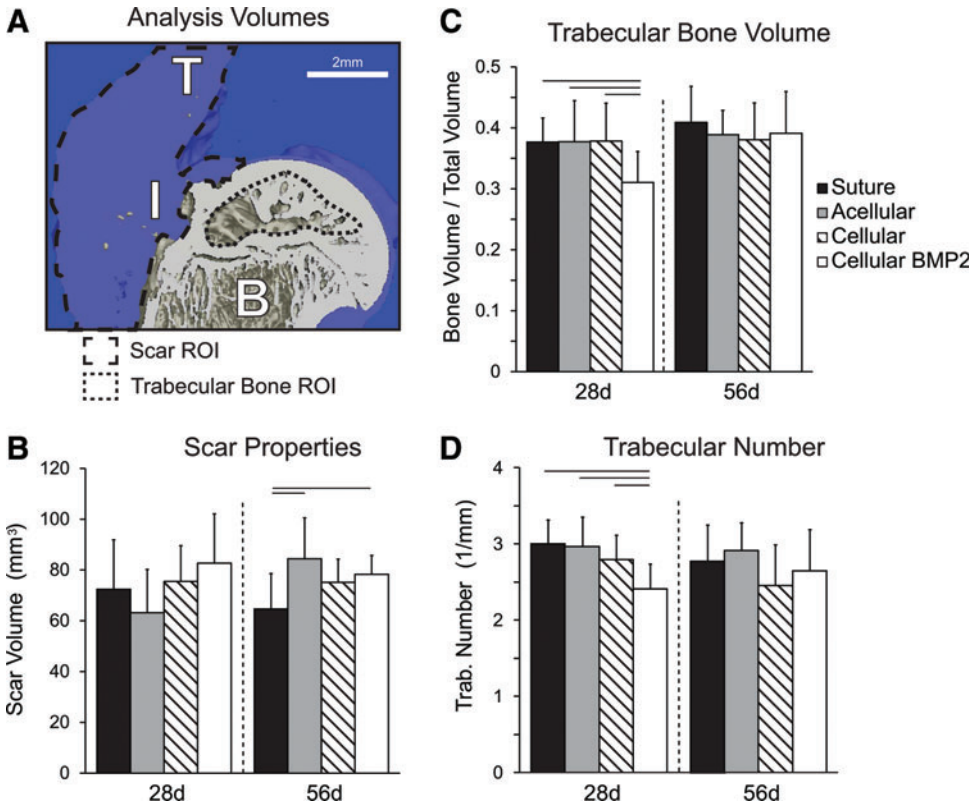

FIG. 3. **(A)** Representative 3D reconstruction of repaired attachment. Regions of analysis are indicated by the outlined areas. B, bone; I, insertion; T, tendon. **(B)** Scar volume increased from 28 to 56 days in the acellular group and the suture group was lower than the acellular and cellular bone morphogenetic protein 2 (BMP2) group. **(C)** Bone volume over total volume was decreased in the cellular BMP2 group compared to other groups at 28 days, but there was no difference at 56 days. **(D)** Trabecular number was significantly lower in the 28 days cellular BMP2 group compared to the other 28 days groups. *Bars*: mean + SD, *lines over bars* indicate $p < 0.05$. Color images available online at www.liebertpub.com/tea

Table 2. Trabecular Thickness was Significantly Increased with Both Time and Cells, Trabecular Spacing was Significantly Increased with Cells

Time point (days)	*Group*	*Tb.Th. (μm)*	*Tb.S. (μm)*	*BMD (mg HA/ccm)*	*Ultimate load (N)*	*Stiffness (N/mm)*	*Ultimate strain (%)*	*Toughness (MPa)*
28	Suture	129 ± 16	331 ± 34[a]	890 ± 26	21 ± 5.5	21.4 ± 6.1	34 ± 14	0.58 ± 0.29
Acellular		127 ± 18	342 ± 57[b]	907 ± 12	25 ± 5.9	18.3 ± 3.9	39 ± 29	0.70 ± 0.37
Cellular		135 ± 17	364 ± 46[c]	902 ± 24	25.7 ± 9.4	19.4 ± 8.9	42 ± 11	0.95 ± 1.11
Cellular BMP2		130 ± 9	424 ± 65[a,b,c]	907 ± 10	19.7 ± 5.9	16.3 ± 3.1	42 ± 16	0.51 ± 0.33
56	Suture	147 ± 26	371 ± 68	907 ± 16	32.3 ± 4.9	31.9 ± 7.5[a]	31 ± 8[a]	1.00 ± 0.7
Acellular		134 ± 18[a]	349 ± 44[a]	900 ± 28	31.1 ± 9.4	25.9 ± 10	34 ± 7[b]	0.82 ± 0.37
Cellular		160 ± 19[a]	423 ± 97[a]	911 ± 13	31.7 ± 10	25.6 ± 9.4	38 ± 11	0.82 ± 0.43
Cellular BMP2		145 ± 21	400 ± 94	917 ± 19	32.6 ± 6.6	24.4 ± 8.3[a]	50 ± 20[a,b]	0.89 ± 0.31

Stiffness and ultimate load were significantly increased with time. Matching superscript letters indicate groups that are significantly different from each other ($p < 0.05$).

BMD, bone mineral density; Tb.S., trabecular separation; Tb.Th., trabecular thickness.

cells that were fibroblasts, cell and collagen orientation, and insertion morphology and continuity were higher (i.e., further from normal) in the scaffold-containing groups compared to the suture-only group at 28 days (Table 1). There were few other apparent differences among groups for the outcomes measured.

Bone and scar tissue morphology

The cellular BMP2 group had significantly lower trabecular bone volume and trabecular number, as well as significantly higher trabecular spacing than the other three treatment groups at 28 days (Fig. 3 and Table 2). The cellular group had significantly higher trabecular thickness than the acellular group at 56 days; however, the cellular group also had significantly increased trabecular spacing than the acellular group at this time point (Table 1). BMD was not significantly different among treatment groups at either time points. When examining changes over time, bone volume and trabecular thickness were significantly increased and the trabecular number was significantly decreased from 28 to 56 days (Fig. 3 and Table 2). BMD and trabecular spacing were not significantly changed with time.

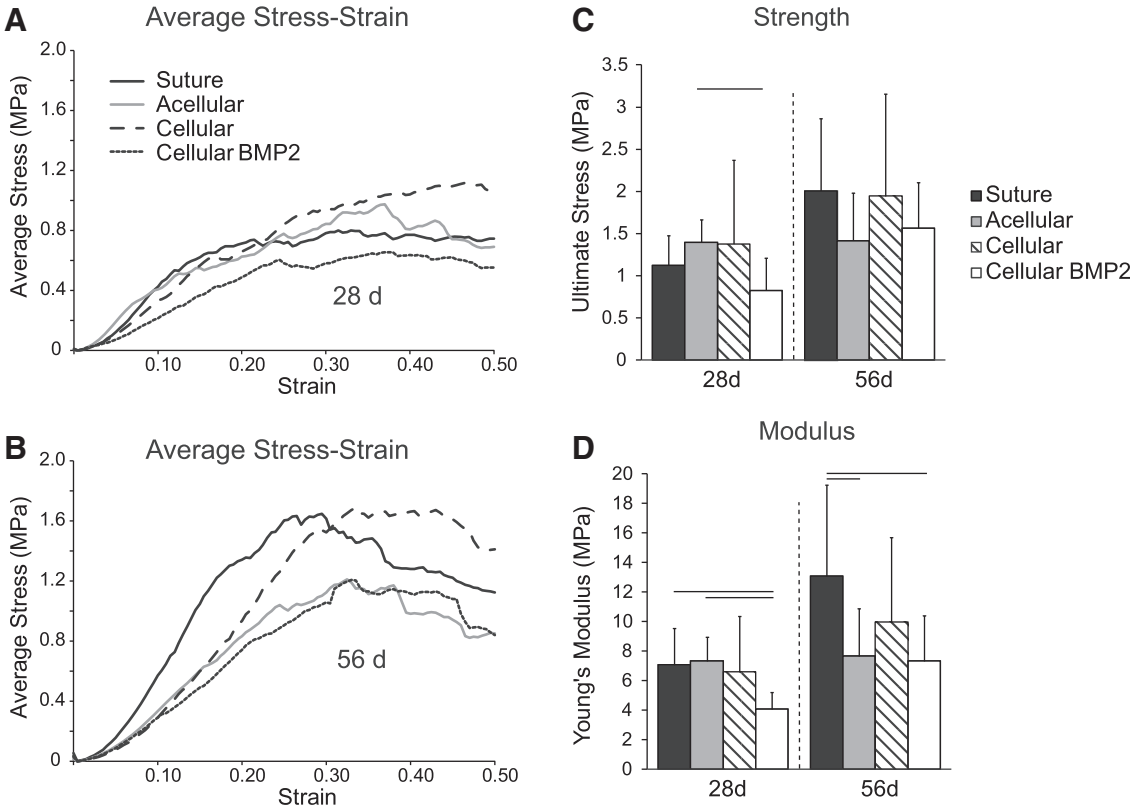

FIG. 4. **(A)** Average stress–strain curves for 28 days groups and **(B)** 56 days groups. **(C)** Ultimate stress (i.e., strength) increased significantly from 28 to 56 days, and decreased due to BMP2 treatment. **(D)** Modulus was lower in the BMP2 group compared to the suture group. Modulus was lower in the acellular group compared to the suture group at 56 days. *Bars*: mean + SD, *lines over bars* indicate $p < 0.05$.

MicroCT was also used to determine the volume of the scar tissue at the healing attachment (Fig. 3A). Scar volume at 28 days was not different among treatment groups. Scar volume at 56 days was significantly increased in acellular and cellular BMP2 groups compared to the suture (control) group. Scar volume was not significantly affected by time.

Mechanical testing

The shapes of the stress–strain curves were similar between groups at each time point, demonstrating initial toe regions, followed by linear regions, followed by yield and postfailure regions (Fig. 4). Strength was significantly decreased in the cellular BMP2 group compared to the acellular group at 28 days (Fig. 4). Modulus was significantly decreased in the cellular BMP2 group compared to the suture and acellular groups at 28 days and compared to the suture group at 56 days (Fig. 4). Modulus was also significantly decreased in the acellular scaffold group compared to the suture (control) group at 56 days. Stiffness was significantly lower in the BMP2 group compared to the suture group at 56 days. The ultimate strain was significantly higher in the BMP2 group compared to the suture and acellular scaffold groups at 56 days. Ultimate load and toughness were not significantly different among treatment groups (Table 2). Structural (stiffness and ultimate load) and material properties (modulus and strength) were significantly increased with time (Fig. 4 and Table 2). Ultimate strain and toughness were not affected by time (Table 2).

Discussion

A nanofiber scaffold with a gradient in mineral was used to deliver cells to the rotator cuff repair site in an animal model. This approach attempted to address two features of failed rotator cuff tendon-to-bone healing: loss of bone and disorganized (scar) matrix formation at the interface. Despite the use of a scaffold mimicking the mineral gradient and aligned nature of the native tendon-to-bone attachment, the repair was dominated by scar formation. Furthermore, the use of cells transduced with the osteogenic factor BMP2 led to impaired healing, as demonstrated by decreased trabecular bone and decreased mechanical properties.

Healing after an acute rotator cuff injury and repair progresses from an early inflammatory phase (on the order of days) to a proliferative and remodeling phase (on the order of weeks), leading to disorganized scar tissue formation composed of types I and III collagen.[3] Although a large volume of scar is deposited at the repair site during healing, the mechanical properties of the attachment remain dramatically lower than the healthy attachment.[3,7] The scar-mediated response is driven by fibroblasts, presumably recruited by inflammatory cytokines.[22] Despite the existence of tendon stem cells,[23] the tendon healing response is scar mediated rather than regenerative. In the current study, ASCs were delivered to the repair site in an effort to promote a regenerative response (i.e., recreation of the native attachment site structure) rather than the natural fibrovascular scar response. Mesenchymal stem cells have been shown to modulate inflammation and differentiate down the multiple lineages, including the tendon fibroblasts, chondrocytes, and osteoblasts found at the healthy tendon-to-bone attachment.[19,20,24] However, delivery of ASCs was ineffective in improving the repair in the current study. The lack of effect may have been due to a low number of implanted cells relative to the numbers of cells that naturally fill the repair site. Moreover, the implanted cells were placed as a patch over the repair site, and therefore were not directly at the interface between the healing tendon and bone.

The scaffold had a negative effect on healing, as demonstrated by decreased mechanical properties. Scaffolds of various types have been used for tissue engineering of the enthesis, including natural materials such as collagen, fibrin, and polymeric materials such as PLGA and poly-lactic acid.[25–27] *In vitro* studies have shown great promise for the use of electrospun polymer scaffolds in tendon-to-bone tissue engineering applications.[28,29] Moffat *et al.* showed that aligned nanofiber scaffolds drove mesenchymal stem cells toward a tendon lineage, ideal for rotator cuff repair. Liu *et al.* showed that a gradient in mineral promoted a gradient in cell phenotype, with osteoblastic differentiation correlating with mineral content.[15] However, few studies have applied these *in vitro* results to a clinically relevant *in vivo* animal model. In the current study, we found that the native fibrovascular response overwhelmed any benefit of the implanted cells or the aligned nanofibers with a gradient in mineral. Indeed, the scaffold itself impaired the healing process, perhaps due to negative effects of PLGA degradation products (e.g., an acidic local environment can potentiate bone loss).[30] A histologic assessment indicated that groups with a scaffold had maturity scores further from normal at 28 days than the group without a scaffold. This corresponds well with the observed decrease in modulus in scaffold-containing groups, since the histology indicated a muted remodeling response in those groups.

Although it is a potent osteogenic agent in most cases, BMP2 has also been shown to cause bone loss in certain cases.[31–33] The delivery of BMP2 through adenoviral gene transfer in the current study led to loss of bone and decreased mechanical properties of the healing tendon-to-bone attachment. Based on BMP2-YFP expression patterns, *in vitro* and *in vivo* studies demonstrated prolonged expression of BMP2. This sustained expression of BMP2 may have led to a negative osteoblast–osteoclast feedback loop and increased bone resorption. BMP2 appears to function in both osteoblastogenesis and osteoclastogenesis, complicating its role as a therapeutic osteogenic growth factor.[31,32] A previous study using recombinant BMP2 in a canine flexor tendon-to-bone repair model also showed an increased resorption and decreased mechanical properties with the use of the growth factor.[33] As osteoclasts are prominent at the healing tendon-to-bone interface and BMP2-stimulated osteoclastogenesis by osteoblast activation, the use of BMP2 for enhanced tendon-to-bone repair is not advised. These results are in contrast to previous studies demonstrating an increased bone formation with BMP2 treatment. For example, delivery of recombinant BMP2 led to the improved healing of a tendon graft in a bone tunnel in an animal model of anterior cruciate ligament reconstruction.[34] This and other positive results using BMP2 imply that the context, delivery method, and dosage of BMP2 may dictate its efficacy. In the current study, BMP2 was delivered using a gene delivery approach,

leading to a sustained, but uncontrolled dosage. It is possible that a different dose of BMP2 may have been more effective in improving tendon-to-bone healing.

There were a number of limitations to the study. First, an empty viral vector control group was not included in the study design. BMP2 was delivered using a viral vector, which could potentially cause an immune reaction. However, the cells were transduced *in vitro*, before implantation, and did not carry adenovirus after transfer. These cells did carry truncated adenovirus genome DNA at implantation, but the genome DNA is not equivalent to virus since the recombinant virus DNA will not amplify anymore. Therefore, it was not expected that the viral delivery method would have any negative effects on healing.

Although the mineral gradient of the scaffold mimics the trend found in the natural insertion, the scale of its length is different. The tendon transitions to bone over hundreds of microns, but the mineral gradient in rodents only spans $\sim 20\,\mu m$.[13] In the current study, the length of the mineral gradient was an order-of-magnitude longer than the natural mineral gradient. This increased length of the mineral gradient may therefore have been ineffective for enhancing the tendon-to-bone repair strength.

In summary, the current study revealed a number of critical considerations for enhancing tendon-to-bone healing using regenerative medicine approaches: (i) regenerative strategies can be overwhelmed by the natural scar-mediated response, (ii) BMP2 is not an effective growth factor for improving tendon-to-bone healing, and (iii) scaffolding material may negatively affect healing.

Acknowledgments

This work was supported, in part, by grants from the National Science Foundation (CAREER 844607 to S.T.) and the National Institutes of Health (DP1OD000798 to Y.X., AR060820 to Y.X. and S.T., and AR057836 to S.T. and L.M.G.). Histology was performed at the Washington University Musculoskeletal Research Center, supported by NIH P30 AR057235.

Disclosure Statement

No competing financial interests exist.

References

1. Pedowitz, R.A., Yamaguchi, K., Ahmad, C.S., Burks, R.T., Flatow, E.L., Green, A., Iannotti, J.P., Miller, B.S., Tashjian, R.Z., Watters, W.C., Weber, K., Turkelson, C.M., Wies, J.L., Anderson, S., St. Andre, J., Boyer, K., Raymond, L., Sluka, P., and McGowan, R. Optimizing the management of rotator cuff problems. J Am Acad Orthop Surg **19,** 368, 2011.
2. Cole, B.J., McCarty Iii, L.P., Kang, R.W., Alford, W., Lewis, P.B., and Hayden, J.K. Arthroscopic rotator cuff repair: prospective functional outcome and repair integrity at minimum 2-year follow-up. J Shoulder Elbow Surg **16,** 579, 2007.
3. Galatz, L.M., Sandell, L.J., Rothermich, S.Y., Das, R., Mastny, A., Havlioglu, N., Silva, M.J., and Thomopoulos, S. Characteristics of the rat supraspinatus tendon during tendon-to-bone healing after acute injury. J Orthop Res **24,** 541, 2006.
4. Harryman, D.T., Mack, L.A., Wang, K.Y., Jackins, S.E., Richardson, M.L., and Matsen, F.A. Repairs of the rotator cuff. Correlation of functional results with integrity of the cuff. J Bone Joint Surg Am **73,** 982, 1991.
5. Galatz, L.M., Ball, C.M., Teefey, S.A., Middleton, W.D., and Yamaguchi, K. The outcome and repair integrity of completely arthroscopically repaired large and massive rotator cuff tears. J Bone Joint Surg Am **86-A,** 219, 2004.
6. Galatz, L.M., Rothermich, S.Y., Zaegel, M., Silva, M.J., Havlioglu, N., and Thomopoulos, S. Delayed repair of tendon to bone injuries leads to decreased biomechanical properties and bone loss. J Orthop Res **23,** 1441, 2005.
7. Thomopoulos, S., Williams, G.R., and Soslowsky, L.J. Tendon to bone healing: differences in biomechanical, structural, and compositional properties due to a range of activity levels. J Biomech Eng **125,** 106, 2003.
8. Killian, M.L., Cavinatto, L., Shah, S.A., Sato, E.J., Ward, S.R., Havlioglu, N., Galatz, L.M., and Thomopoulos, S. The effects of chronic unloading and gap formation on tendon-to-bone healing in a rat model of massive rotator cuff tears. J Orthop Res **32,** 439, 2014.
9. Galatz, L.M., Charlton, N., Das, R., Kim, H.M., Havlioglu, N., and Thomopoulos, S. Complete removal of load is detrimental to rotator cuff healing. J Shoulder Elbow Surg **18,** 669, 2009.
10. Cadet, E.R., Vorys, G.C., Rahman, R.K., Park, S.-H., Gardner, T.R., Lee, F.Y., Levine, W.N., Bigliani, L.U., and Ahmad, C.S. Improving bone density at the rotator cuff footprint increases supraspinatus tendon failure stress in a rat model. J Orthop Res **28,** 308, 2010.
11. Wozney, J.M., Rosen, V., Celeste, A.J., Mitsock, L.M., Whitters, M.J., Kriz, R.W., Hewick, R.M., and Wang, E.A. Novel regulators of bone formation: molecular clones and activities. Science **242,** 1528, 1988.
12. McKay, W.F., Peckham, S.M., and Badura, J.M. A comprehensive clinical review of recombinant human bone morphogenetic protein-2 (INFUSE® Bone Graft). Int Orthop **31,** 729, 2007.
13. Schwartz, A.G., Pasteris, J.D., Genin, G.M., Daulton, T.L., and Thomopoulos, S. Mineral distributions at the developing tendon enthesis. PLoS One **7,** e48630, 2012.
14. Li, X., Xie, J., Lipner, J., Yuan, X., Thomopoulos, S., and Xia, Y. Nanofiber scaffolds with gradations in mineral content for mimicking the tendon-to-bone insertion site. Nano Lett **9,** 2763, 2009.
15. Liu, W., Lipner, J., Xie, J., Manning, C.N., Thomopoulos, S., and Xia, Y. Nanofiber scaffolds with gradients in mineral content for spatial control of osteogenesis. ACS Appl Mater Interfaces **6,** 2842, 2014.
16. Manning, C.N., Schwartz, A.G., Liu, W., Xie, J., Havlioglu, N., Sakiyama-Elbert, S.E., Silva, M.J., Xia, Y., Gelberman, R.H., and Thomopoulos, S. Controlled delivery of mesenchymal stem cells and growth factors using a nanofiber scaffold for tendon repair. Acta Biomater **9,** 6905, 2013.
17. Tas, A.C., and Bhaduri, S.B. Rapid coating of Ti6Al4V at room temperature with a calcium phosphate solution similar to 10× simulated body fluid. J Mater Res **19,** 2742, 2004.
18. Qu, X., Cui, W., Yang, F., Min, C., Shen, H., Bei, J., and Wang, S. The effect of oxygen plasma pretreatment and incubation in modified simulated body fluids on the

formation of bone-like apatite on poly(lactide-co-glycolide) (70/30). Biomaterials **28,** 9, 2007.
19. Shen, H., Gelberman, R.H., Silva, M.J., Sakiyama-Elbert, S.E., and Thomopoulos, S. BMP12 induces tenogenic differentiation of adipose-derived stromal cells. PLoS One **8,** e77613, 2013.
20. Gimble, J., and Guilak, F. Adipose-derived adult stem cells: isolation, characterization, and differentiation potential. Cytotherapy **5,** 362, 2003.
21. Yokoya, S., Mochizuki, Y., Nagata, Y., Deie, M., and Ochi, M. Tendon-bone insertion repair and regeneration using polyglycolic acid sheet in the rabbit rotator cuff injury model. Am J Sports Med **36,** 1298, 2008.
22. Bunker, D.L.J., Ilie, V., Ilie, V., and Nicklin, S. Tendon to bone healing and its implications for surgery. Muscles Ligaments Tendons J **4,** 343, 2014.
23. Bi, Y., Ehirchiou, D., Kilts, T.M., Inkson, C.A., Embree, M.C., Sonoyama, W., Li, L., Leet, A.I., Seo, B.-M., Zhang, L., Shi, S., and Young, M.F. Identification of tendon stem/progenitor cells and the role of the extracellular matrix in their niche. Nat Med **13,** 1219, 2007.
24. Erickson, G.R., Gimble, J.M., Franklin, D.M., Rice, H.E., Awad, H., and Guilak, F. Chondrogenic potential of adipose tissue-derived stromal cells in vitro and in vivo. Biochem Biophys Res Commun **290,** 763, 2002.
25. Gulotta, L.V., Kovacevic, D., Packer, J.D., Deng, X.H., and Rodeo, S.A. Bone marrow-derived mesenchymal stem cells transduced with scleraxis improve rotator cuff healing in a rat model. Am J Sports Med **39,** 1282, 2011.
26. Sato, M., Maeda, M., Kurosawa, H., Inoue, Y., Yamauchi, Y., and Iwase, H. Reconstruction of rabbit Achilles tendon with three bioabsorbable materials: histological and biomechanical studies. J Orthop Sci **5,** 256, 2000.
27. Davis, P.A., Huang, S.J., Ambrosio, L., Ronca, D., and Nicolais, L. A biodegradable composite artificial tendon. J Mater Sci Mater Med **3,** 359, 1992.
28. Mauck, R.L., Baker, B.M., Nerurkar, N.L., Burdick, J.A., Li, W.J., Tuan, R.S., and Elliott, D.M. Engineering on the straight and narrow: the mechanics of nanofibrous assemblies for fiber-reinforced tissue regeneration. Tissue Eng Part B Rev **15,** 171, 2009.
29. Moffat, K.L., Kwei, A.S., Spalazzi, J.P., Doty, S.B., Levine, W.N., and Lu, H.H. Novel nanofiber-based scaffold for rotator cuff repair and augmentation. Tissue Eng Part A **15,** 115, 2009.
30. Fu, K., Pack, D., Klibanov, A., and Langer, R. Visual evidence of acidic environment within degrading poly(lactic-co-glycolic acid) (PLGA) microspheres. Pharm Res **17,** 100, 2000.
31. Abe, E., Yamamoto, M., Taguchi, Y., Lecka-Czernik, B., O'Brien, C.A., Economides, A.N., Stahl, N., Jilka, R.L., and Manolagas, S.C. Essential requirement of BMPs-2/4 for both osteoblast and osteoclast formation in murine bone marrow cultures from adult mice: antagonism by noggin. J Bone Miner Res **15,** 663, 2000.
32. Samee, N., Geoffroy, V., Marty, C., Schiltz, C., Vieux-Rochas, M., Levi, G., and de Vernejoul, M.-C. Dlx5, a positive regulator of osteoblastogenesis, is essential for osteoblast-osteoclast coupling. Am J Pathol **173,** 773, 2008.
33. Thomopoulos, S., Kim, H.M., Silva, M.J., Ntouvali, E., Manning, C.N., Potter, R., Seeherman, H., and Gelberman, R.H. Effect of bone morphogenetic protein 2 on tendon-to-bone healing in a canine flexor tendon model. J Orthop Res **30,** 1702, 2012.
34. Rodeo, S.A., Suzuki, K., Deng, X.H., Wozney, J., and Warren, R.F. Use of recombinant human bone morphogenetic protein-2 to enhance tendon healing in a bone tunnel. Am J Sports Med **27,** 476, 1999.

Address correspondence to:
Stavros Thomopoulos, PhD
Department of Orthopedic Surgery
Columbia University
Black Building 1408
650 W 168 Street
New York, NY 10032

E-mail: sat2@columbia.edu

Received: March 4, 2015
Accepted: August 28, 2015
Online Publication Date: October 13, 2015